A&A 373, 816–826 (2001)
DOI: 10.1051/0004-6361:20010651


Astronomy & Astrophysics

# A near-solar metallicity damped Lyman-$\alpha$ system toward the BAL quasar Tol 1037−2703⋆

R. Srianand[1] and P. Petitjean[2,3]

[1] IUCAA, Post Bag 4, Ganeshkhind, Pune 411 007, India
[2] Institut d'Astrophysique de Paris – CNRS, 98bis Boulevard Arago, 75014 Paris, France
[3] UA CNRS 173 – DAEC, Observatoire de Paris-Meudon, 92195 Meudon Cedex, France

Received 6 February 2001 / Accepted 23 April 2001

**Abstract.** We report the detection of a Broad Absorption Line (BAL) outflow in the spectrum of the $z_{\rm em}$ (Mg II) = 2.201 QSO Tol 1037−2703 with three main BALs at 36 000, 25 300 and 22 300 km s$^{-1}$ outflow velocities. Although the overall flow is dominated by high ionization lines like N V and C IV, the gas of highest velocity shows absorption from Mg I, Mg II and Fe II. Covering factor arguments suggest that the absorbing complexes are physically associated with the QSO and have transverse dimensions smaller than that of the UV continuum emitting region ($r < 0.1$ pc). We show that the C IV absorption at $z_{\rm abs} = 2.082$ has a covering factor $f_{\rm c} \sim 0.86$ and the absorption profile has varied over the last four years. The detection of absorption from excited fine structure levels of C II and Si II in narrow components embedded in the C IV trough reveals large density inhomogeneities. IR pumping is the most likely excitation process. The $z_{\rm abs} = 2.139$ system is a moderately damped Lyman-$\alpha$ system with log $N$(H I) $\sim$ 19.7. The weakness of the metal lines together with the high quality of the data make the metallicity measurements particularly reliable. The absolute metallicity is close to solar with [Zn/H] = −0.26. The $\alpha$-chain elements have metallicities consistently solar (respectively +0.05, −0.02, −0.03 and −0.15 for [Mg/H], [Si/H], [P/H] and [S/H]) and iron peak elements are depleted by a factor of about two ([Fe/Zn], [Cr/Zn], [Mn/Zn] and [Ni/Zn] are equal to −0.39, −0.27, −0.49, −0.30). Lines from C I are detected but $H_2$ is absent with a molecular to neutral hydrogen fraction less than $8\times10^{-6}$. From the ionization state of the gas, we argue that the system is situated ∼few Mpc away from the QSO. High metallicity and low nitrogen abundance, [N/Zn] = −1.40, favor the idea that metals have been released by massive stars during a starburst of less than 0.5 Gyr of age. Using the upper limit on the C I* column density in two components, we obtain upper limits on the background temperature of 16.2 and 13.2 K respectively.

**Key words.** galaxies: intergalactic medium – galaxies: quasars: absorption lines

## 1. Introduction

The remarkable similarity of four C IV absorption systems at redshift $1.95 < z_{\rm abs} < 2.14$ in the spectra of Tol 1037−2703 ($z_{\rm em} = 2.20$) and 1038−2712 ($z_{\rm em} = 2.33$) separated by only 17.9 arcmin on the sky has created considerable interest in the past. However the nature and origin of these common absorption systems are still unclear. There are arguments as well as counter arguments for (i) the absorption being produced by a super−cluster sitting in front of the two quasars and (ii) part of the systems being intrinsically associated with the QSOs (see Jakobsen et al. 1986; Ulrich & Perryman 1986; Cristiani et al. 1987; Robertson 1987; Sargent & Steidel 1987; Dinshaw & Impey 1996; Lespine & Petitjean 1997).

Here we use a high resolution and high $S/N$ ratio spectrum of Tol 1037−2703 of quality an order of magnitude higher than previous data to investigate the nature of the systems close to the quasar redshift, mainly the broad outflow and the systems at $z_{\rm abs} \sim 2.082$ and 2.139. As it is now established that the absorbing gas physically associated with the QSOs often shows some or all of: (i) partial coverage, (ii) excited fine-structure lines, (iii) time variability, (iv) broader albeit smoother profile, (v) high metal enrichment (see e.g. Petitjean et al. 1994; Hamann 1997; Petitjean & Srianand 1999; Srianand & Petitjean 2000), we can investigate the nature of these systems using these indicators.

Observations are described in Sect. 2. Section 3 presents the spectral energy distribution and accurate redshift of the QSO. We discuss the BAL flow in Sect. 4 and study the nature of the $z_{\rm abs} \sim 2.082$ and 2.139 C IV systems in greater detail in Sect. 5. The results are summarized and discussed in Sect. 6.

*Send offprint requests to*: R. Srianand,
e-mail: anand@iucaa.ernet.in

⋆ Based on observations collected during ESO programme 65.P-0038 at the European Southern Observatory with UVES mounted on the 8.2 m KUEYEN telescope operated on Cerro Paranal, Chile.

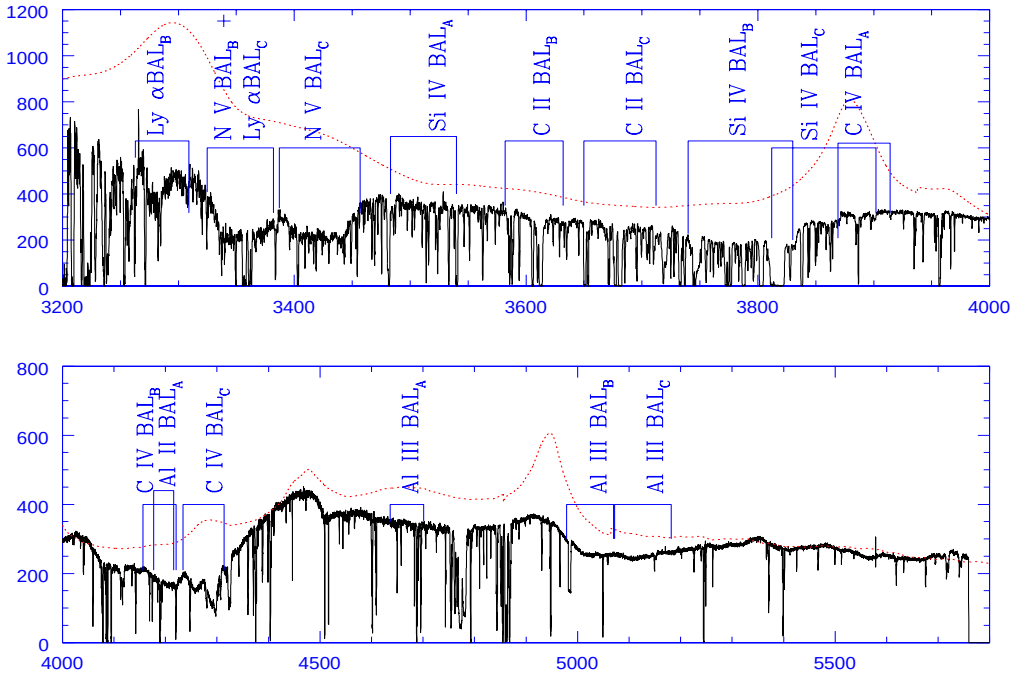


**Fig. 1.** Portion of the Tol 1037−2703 spectrum. A high-quality UVES spectrum of Q1101−264 shifted in wavelength and intensity is overplotted (dotted line). Position of various BALs discussed in the text are indicated. The subscripts "A", "B" and "C" denote the $z_{\rm abs}$ = 1.51, 1.70 and 1.75 systems respectively.

## 2. Observations

The Ultra-violet and Visible Echelle Spectrograph (D'Odorico et al. 2000) mounted on the ESO Kueyen 8.2 m telescope at the Paranal observatory was used on April 5 to 8, 2000 to obtain high-spectral resolution spectra of Tol 1037−2703. The slit width was 1 arcsec (the seeing $FWHM$ was most of the time better than 0.8 arcsec) and the CCDs were binned 2×2 resulting in a resolution of ∼45 000. The total exposure time ∼9 hours was split into 1 h exposures. The data were reduced in the dedicated context of MIDAS, the ESO data reduction package, using the UVES pipeline in an interactive mode. The main characteristics of the pipeline are to perform a precise inter-order background subtraction for science frames and master flat-fields, and an optimal extraction of the object signal rejecting cosmic ray impacts and subtracting the sky at the same time. The reduction is checked step by step. Wavelengths were corrected to vacuum-heliocentric values and individual 1D spectra were combined together. The resulting $S/N$ ratio per pixel is of the order of 20 at ∼3500 Å and 40 at ∼6000 Å.

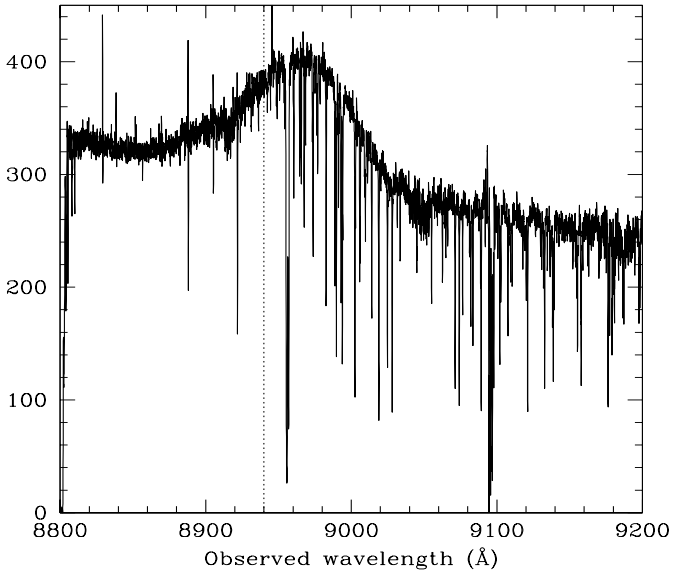


**Fig. 2.** The Mg II emission line of Tol 1037−2703 at a redshift of $z$ = 2.201. The vertical dotted line marks the expected position the emission line for the $z_{\rm em}$ = 2.14 redshift defined by high ionization emission lines.

## 3. BAL flow and emission redshift

Part of the observed spectrum of Tol 1037−2703 is shown in Fig. 1. For comparison we have also plotted the suitably shifted continuum of Q 1101−264. It is apparent that most of the emission lines are weak due to numerous broad absorption troughs. Expected positions of various absorption lines due to three BALs are marked. These systems are discussed in detail in the next section.

Unlike most of the other emission lines, Mg II emission is clearly seen in our red spectrum (see Fig. 2). This provides us with the accurate measurement of the emission redshift of the QSO, $z_{\rm em}$ = 2.201, which is important for the study of associated systems. Jakobsen et al. (1986) have measured $z_{\rm em}$ = 2.193 from the high excitation emission lines, which is 2400 km s$^{-1}$ smaller than our determination. Gaskell (1982) has shown, however, that there is a systematic difference between the redshifts

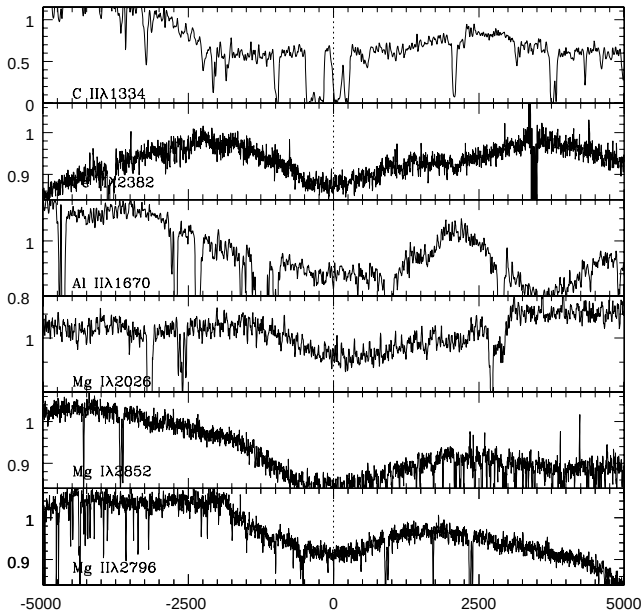


**Fig. 3.** Velocity plot of broad absorption lines from the $z_{\rm abs} = 1.5181$ system.

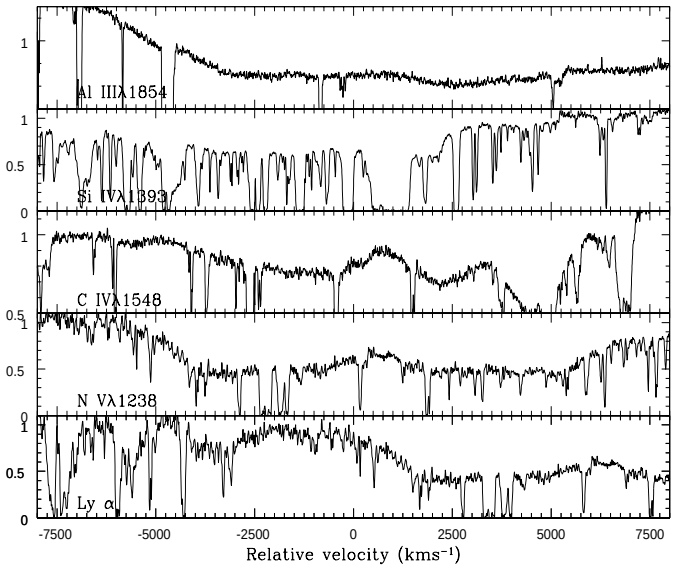


**Fig. 4.** Velocity plot of broad absorption lines in the twin BAL system at $z_{\rm abs} = 1.7018$ and 1.7569.

derived from broad emission-lines of different ionization levels. The mean blue-shift of C IV, N V and possibly Lyman-$\alpha$ with respect to low-ionization lines as O I, Mg II and the Balmer lines is about 600 km s$^{-1}$ (Espey et al. 1989). The corresponding blueshift for Tol 1037−2703 is larger than this but not exceptional.

## 4. Broad absorption systems

### 4.1. $z_{abs} = 1.5181$

This system is identified by broad absorption lines of Mg II$\lambda$2800 and Mg I$\lambda$2852. Presence of Fe II$\lambda$2382, Fe II$\lambda$2600 and possibly Mg I$\lambda$2026 in the red spectrum (see Fig. 3) confirms the identification. Note that the unidentified line in the low resolution spectrum of Ulrich & Perryman (1986) correspond to Fe II at this redshift (see their Fig. 1). The Mg II absorption trough has $FWHM \sim$ 2400 km s$^{-1}$ and ejection velocity 36 000 km s$^{-1}$ with respect to the QSO. Absorption lines due to Al II$\lambda$1670 and Si II$\lambda$1304 could be present. The Al II line is probably blended with C IV absorption at $z_{\rm abs} = 1.7$ (see below). Si II$\lambda$1526 and C IV absorptions are redshifted on top of the QSO Lyman-$\alpha$ +N V emission line and could possibly be responsible for the weakness of the emission feature. The expected position of C II$\lambda$1334 coincides with the broad feature at 3360 Å, together with Lyman-$\alpha$ and N V BALs at $z_{\rm abs} = 1.76$ (see below). Blending with the intervening Lyman-$\alpha$ absorption lines and other broad absorption troughs prevents systematic estimate of column densities.

The so-called low ionization Mg II BALs are seen in 15% of the BALQSOs detected in optical surveys (Voit et al. 1993). All the known Mg II BAL systems have strong absorption due to C IV, Al II and Al III; the absorption due to Al III being prominent compared to that of Al II. The profiles of low ionization BALs are always shallower and narrower than that of high ionization transitions (Voit et al. 1993). Becker et al. (2000) have suggested that the fraction of BALs amongst radio selected QSOs are high and ∼50% of them show absorption due to low ionization species. It is interesting to note that no BAL due to Mg I has been mentioned up to now (see however de Kool et al. 2001).

After carefully taking into account the atmospheric features, the Mg I$\lambda$2852 rest equivalent width is $w_{\rm r} =$ 0.78 Å and $FWHM = 1523$ km s$^{-1}$. Correspondingly, $w_{\rm r}$(Mg II) is 2.35 Å. This gives $N$(Mg II) $\geq 4 \times 10^{13}$ and $N$(Mg I) $\geq 1 \times 10^{14}$ cm$^{-2}$. As the ionization potential of Mg I is less than 13.6 eV, even if hydrogen is completely neutral, $N$(Mg II) is expected and observed to be larger than $N$(Mg I). This strongly suggests that the absorbing gas does not completely cover the background source. From the residual intensities we estimate that the covering factor could be as low as ∼0.1 which would be consistent with the strength of the Fe II lines. The Mg II absorption is redshifted in a region devoid of any emission line. This means the absorbing gas has a projected size of less than 0.01 pc (10% of the typical size of the UV continuum emitting region). It must be noted that the presence of such low covering factor in BAL flows has already been mentioned (Hamann et al. 1997; Telfer et al. 1998; Srianand & Petitjean 2000).

### 4.2. $z_{abs} = 1.7018$ and 1.7569

The twin system is detected mainly through a strong N V through seen at $\lambda_{\rm obs} \sim$ 3400 Å. From Fig. 4 it is apparent that C IV absorption is present in both components. Although not excluded, it is unclear whether Si IV and Al III absorption lines are present. It is interesting to note that the bottom of the N V absorption is flat for both components but without going to zero. Continuum in this wavelength range is not well defined however (see Fig. 1).

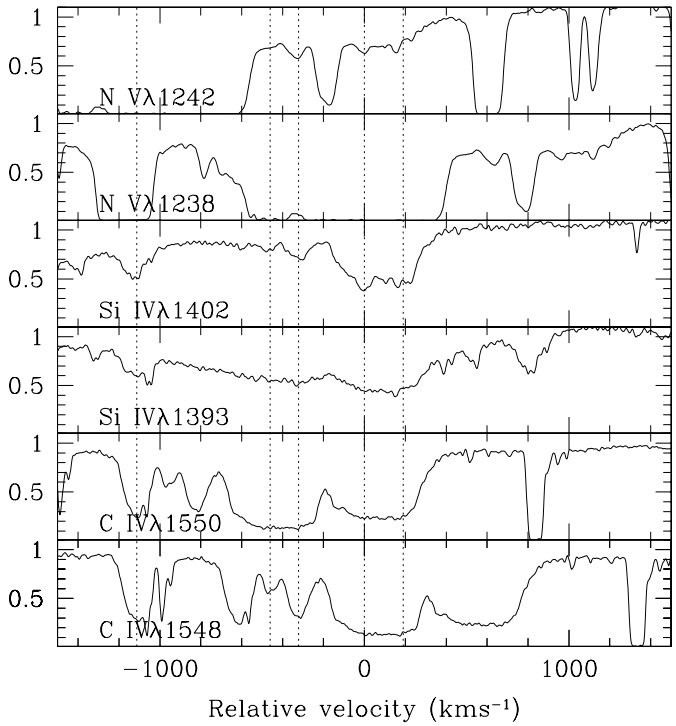


**Fig. 5.** Velocity plot of high ionization lines from the $z_{\rm abs} = 2.082$ system. The vertical dotted lines mark some of the components discussed in the text.

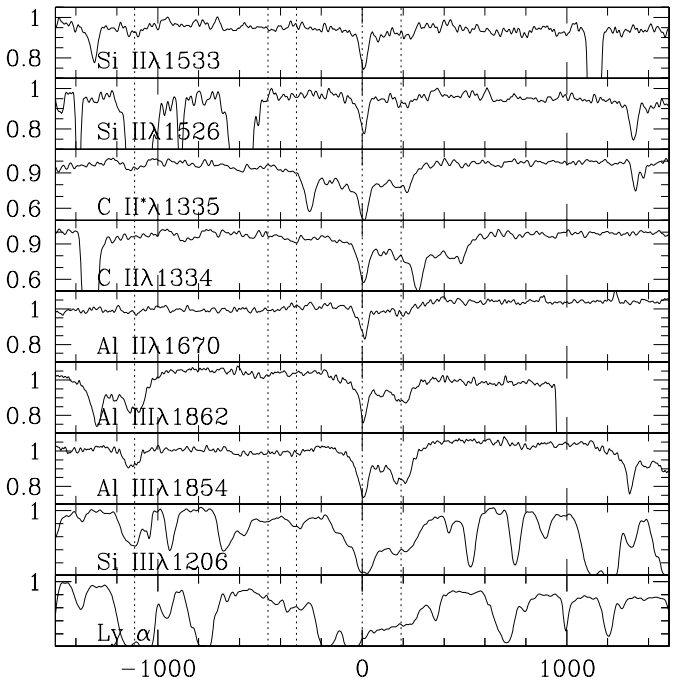


**Fig. 6.** Velocity plot of low ionization lines from the $z_{\rm abs} = 2.082$ system. The vertical dotted lines mark some of the components discussed in the text. The main narrow component is at $z_{\rm abs} = 2.0819$.

Therefore, by fitting the continuum locally we find that the residual intensity is ∼0.5, suggesting the covering factor of N V could be close to 0.5. If we normalise the spectrum by fitting the regions free from absorption to the Q 1101−264 spectrum, we derive a covering factor of ∼0.7. As the N V lines are saturated we obtain tentative lower limits on the N V column densities, $\geq 3.4 \times 10^{16}$ and $\geq 4.0 \times 10^{16}$ cm$^{-2}$ respectively for the two components. The $FWHM$ are ∼4000 km s$^{-1}$ and ∼6000 km s$^{-1}$ respectively. These components are at an ejection velocity of 25 300 and 22 320 km s$^{-1}$ with respect to the QSO redshift defined by the Mg II emission.

The absence of absorption due to singly ionized species, the weakness of the H I Lyman-$\alpha$ line and the fact that N V is stronger than C IV suggest that ionization conditions in these systems are similar to those of standard high-ionization BALs. Assuming the nitrogen abundance to be ten times solar and N V to be the dominant nitrogen species we estimate a lower limit on the total hydrogen column density of $3.9{\times}10^{19}$ and $4.2{\times}10^{19}$ cm$^{-2}$ for the two components. The observed upper limit on $N$(H I) at $z_{\rm abs} = 1.7018$ is $10^{15}$ cm$^{-2}$ implying $\log U \geq -1.0$ (Hamann 1997).

### 4.3. $z_{abs} = 2.082$

This system has induced considerable interest among astronomers as there is a similar, albeit diffuse, broad absorption trough at the same redshift in the spectrum of QSO Tol 1038−2712 which is at a projected separation of 17.9 arcmin on the sky (or $\sim 4.5h^{-1}$ Mpc at $z = 2$) from Tol 1037−2703. Whether the gas is associated with the QSO or with an intervening absorption complex is unclear however (see Jakobsen et al. 1986; Ulrich & Perryman 1986; Cristiani et al. 1987; Robertson 1987; Sargent & Steidel 1987; Dinshaw & Impey 1996; Lespine & Petitjean 1997). Absorption profiles of high-ionization lines are shown in Fig. 5. Si IVλ1393 is blended with C IV of the BAL system at $z_{\rm abs} = 1.7569$ (see Fig. 4) and N Vλ1238 is blended with Lyman-$\alpha$ at $z_{\rm abs} = 2.139$ (see Fig. 14). The C IV absorption at $v = 0$ km s$^{-1}$ is broad and unresolved even at our resolution. The relative strength of C IVλ1548 and C IVλ1550 absorption lines suggests that the lines are moderately saturated and the gas covers only part of the background source. As these lines are redshifted in a region devoid of emission lines, the projected size of the absorbing gas has to be less than the typical dimension of the region emitting the continuum.

This component also shows absorption due to low ionization lines such as Al II, Si II, C II, Si III, Al III and absorption due to fine-structure lines of Si II and C II (see Fig. 6). The expected position of Mg IIλ2797 unfortunately coincides with a small gap in our UVES spectrum. The detected low ionization lines have a complex structure with a strong narrow component at $z_{\rm abs} = 2.0819$ superimposed on a diffuse broader profile.

#### 4.3.1. Partial coverage

We estimate the covering factor, $f_{\rm c}$, of the C IV gas using the method described in Srianand & Shankaranarayanan (1999). In the case of unblended doublets one can write

$$f_{\rm c} = \frac{1 + R_2^2 - 2R_2}{1 + R_1 - 2R_2}, \quad (1)$$

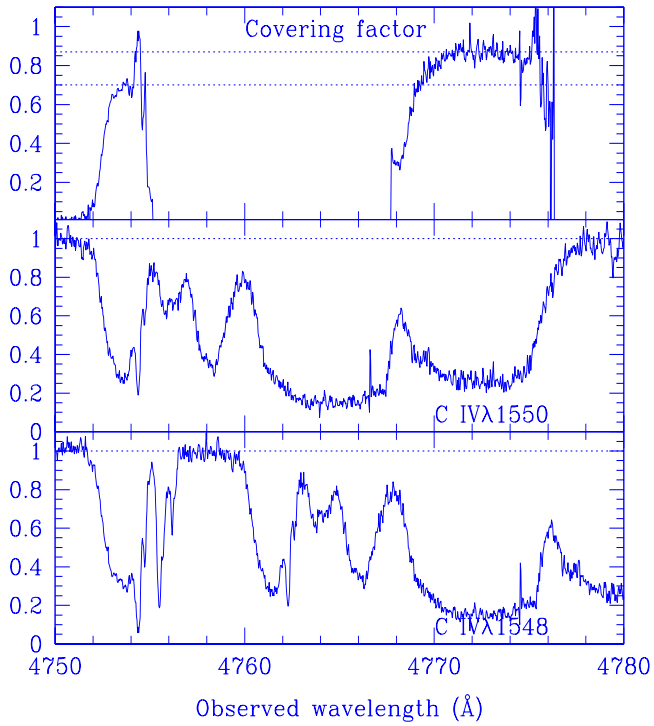


**Fig. 7.** Covering factor estimated from the C IV absorption at $z_{abs} = 2.082$ (top panel). The lower and middle panels give the C IV$\lambda$1548 and C IV$\lambda$1550 profiles (suitably shifted).

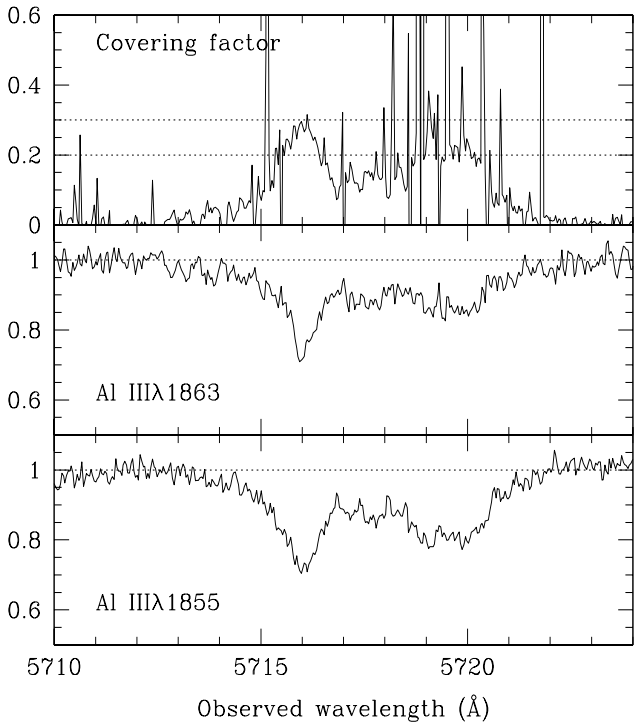


**Fig. 8.** Covering factor estimated from the Al III absorption at $z_{abs} = 2.082$ (top panel). Lower and middle panels give respectively the profiles of Al III$\lambda$1855 and Al III$\lambda$1863 (suitably shifted).

where $R_1$ and $R_2$ are the residual intensities in the first and second lines of the doublet. Typical error in the estimated covering factor is equal to rms in the normalised continuum. As the C IV absorption lines from this system are not contaminated by any broad absorption trough (see Fig. 1) our continuum estimation, based on spline fit, in this wavelength range is reliable. The lower and middle panels of Fig. 7 give the normalised C IV$\lambda$1548 and C IV$\lambda$1550 profiles on a velocity scale. The top panel gives the estimated covering factor. The C IV absorption at $v \sim 0$ km s$^{-1}$ (i.e. $\lambda \sim 4773$ Å) is consistent with a covering factor $f_c = 0.86 \pm 0.03$. It should be noted that C IV$\lambda$1548 of this component has some contamination from C IV$\lambda$1550 of the two narrower C IV$\lambda$1548 components at $\lambda \sim 4764$ and 4766 Å. Taking into account this contamination would decrease the covering factor. Moreover, the fact that the C IV$\lambda$1550 components are not seen superimposed onto the flat bottom of the C IV$\lambda$1548 profile (at $\lambda \sim 4773$ Å) strongly supports the idea that the C IV$\lambda$1548 line is optically thick at this position and $f_c = 0.86$. *This implies as well that the three clouds (with central* C IV$\lambda$1548 *wavelengths at* $\lambda \sim 4764$, *4766 and 4773 Å) must cover the same part of the background source.* This could be a consequence of the absorption arising through a strongly collimated flow.

The estimated covering factor for C IV is constant within the absorption line profile. This suggests that there are no large variations of the line of sight velocity field across the absorbing cloud. The estimated covering factor for the component at $v \sim -1110$ km s$^{-1}$ (i.e. $\lambda \sim 4754$ Å) is $f_c \sim 0.7$. The distinct narrow component in the red wing showing complete coverage probably corresponds to a normal intervening system.

The same analysis is done for the Al III doublet (see Fig. 8) which is not contaminated by any broad absorption trough. In this wavelength range too, the continuum is well approximated by spline fitting. As discussed before, the profile shows a narrow component on top of a broad absorption structure. Within the uncertainties, the covering factor is in the range $\sim$0.2$-$0.3 (see Fig. 8). It is well known, however, that the blending of weak unresolved lines can mimic partial coverage (Lespine & Petitjean 1997). In order to ascertain the above result, we have fitted the Al III doublet with multiple Voigt profile components taking into account the partial coverage. The best fit result is presented in Fig. 9. It is apparent from the figure that, at least for the strongest component, partial covering factor ($f_c \sim 0.3$) is needed. This confirms that the gas responsible for the $z_{abs} = 2.082$ system covers the background source only partially. The estimated covering factor varies from one species to the other, being larger for higher excitation lines (see also Petitjean & Srianand 1999; Srianand & Petitjean 2000).

### 4.3.2. Excited fine-structure lines

It can be seen in Fig. 6 that absorption lines from low-ionization species (C II, Si II and Al II) are present in a well defined narrow component at $z_{abs} = 2.0819$. The presence

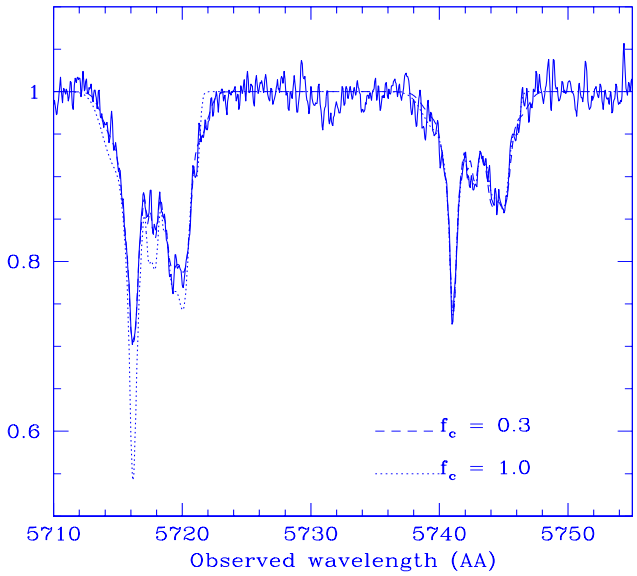


**Fig. 9.** Voigt profile fits to the Al III doublets. The observed (solid line) and model profiles for complete coverage (dotted line) and with 30% coverage (dashed line) are presented.

of strong associated Si II* and C II* lines suggests either that the electron density of the gas is large or that the gas is very close to an IR emitting source.

The observed equivalent widths and profiles of the two lines C II$\lambda$1334 and C II*$\lambda$1335 are similar. Since their rest wavelength and oscillator strengths (0.1278 and 0.1149 respectively) are nearly identical, C II and C II* have about the same column densities, if the lines are not saturated. If we assume electron collisions are responsible for the excitation, the electron density $n_{\rm e}$ is then given by,

$$n_{\rm e} \sim 75\ T_4^{0.5}/[\exp(-91.25/T) - 1]\ {\rm cm}^{-3}, \quad (2)$$

where $T_4$ is the kinetic temperature in units of $10^4$ K. The relevant cross-sections are taken from Bahcall & Wolfe (1968).

From the strength of Si II$\lambda$1526 and Si II*$\lambda$1533, at $z_{\rm abs} = 2.0819$, we derive that the ratio $\beta = N({\rm Si\ II})/N({\rm Si\ II^*})$ is in the range $1.58 < \beta < 2.36$ for a covering factor in the range 0.3−1.0. Note that the above range also includes Voigt profile fitting errors in estimating the individual column densities. Assuming that excitation and de-excitation are due to electron collisions we obtain

$$n_{\rm e} = \frac{1.28 \times 10^3\ T_4^{0.5}}{[2\beta\exp(-413/T) - 1]}{\rm cm}^{-3}. \quad (3)$$

We therefore derive that the electron density is in the range 360−630 cm$^{-3}$ for an assumed temperature of $10^4$ K. This is inconsistent with the density derived from C II. This implies that another excitation mechanism is at play. Note that although it is difficult to estimate the $N({\rm Si\ II})/N({\rm Si\ II^*})$ column density ratio in the broader component, it is consistent with that of the narrow component.

Indeed, excited levels can be populated by IR radiation emitted by the QSOs. In that, case,

$$\frac{N(X^*)}{N(X)} = 2 \times \left(\frac{\bar{n}_\lambda}{1+\bar{n}_\lambda}\right) \quad (4)$$

Where $X$ is either C II or Si II and $\bar{n}_\lambda$ is given by

$$\bar{n}_\lambda = \frac{I(\nu)\lambda^3}{8\pi hc} \quad (5)$$

where $I(\nu)$, in erg cm$^{-2}$ s$^{-1}$ Hz$^{-1}$, is the flux energy density integrated in all directions. From the observed column density ratios we get,

$$\bar{n}_\lambda({\rm C\ II^*}) = (2-4)\bar{n}_\lambda({\rm Si\ II^*}). \quad (6)$$

Such a flux energy density ratio can be achieved by an IR spectrum, $I(\nu) \propto \nu^\alpha$, with $\alpha$ in the range 2 to 2.5. Even though the IR spectrum of Tol 1037−2703 is not known, the required spectral index is typical of what is seen in high redshift QSOs (e.g. Elvis et al. 1994).

Therefore the dominant excitation process is probably pumping by the infrared ambient radiation field and it is not possible to estimate the electronic density from Eqs. (1) and (2). Srianand & Petitjean (2000) reached a similar conclusion to explain the excitation of fine−structure lines in the $z_{\rm abs} = 3.8931$ system toward APM 08279+5255.

### 4.3.3. Variability

If the presence of excited fine-structure lines and the partial covering factor is due to the density of the gas being high, then it is possible, in principle, to constrain the density from variability observations. To investigate this, we use the high-resolution spectrum obtained with the instrument CASPEC on the ESO 3.6 m telescope. This spectrum is the combination of data obtained during two observing runs in December 1992 & April 1994 (see Lespine & Petitjean 1997). This corresponds to an elapsed time of ∼2 yrs in the rest frame of the QSO compared to the new UVES data. The CASPEC data has slightly lower resolution and has inherent problems with background subtraction due to small inter-order spacing in the blue. We therefore have convolved the UVES spectrum with a Gaussian profile to match the width of the narrow lines in the CASPEC spectrum. We have corrected for the background inaccuracy by matching the depth of the narrow lines due to intervening systems which are present close to the C IV absorption at $\lambda$4744 and $\lambda$4893 (see Fig. 10). From Fig. 10, it is clear that, while the narrow lines in both spectra are identical, the broad lines covering the observed wavelength range 4750−4790 Å have become stronger with time. In addition, the shape of the broadest component has changed. This variability is confirmed in a MMT spectrum taken in 1994 (Dinshaw & Impey 1996). We do not see any variation in the relative position of the different components suggesting that acceleration is small. Note however that the narrow Si II absorption lines did not

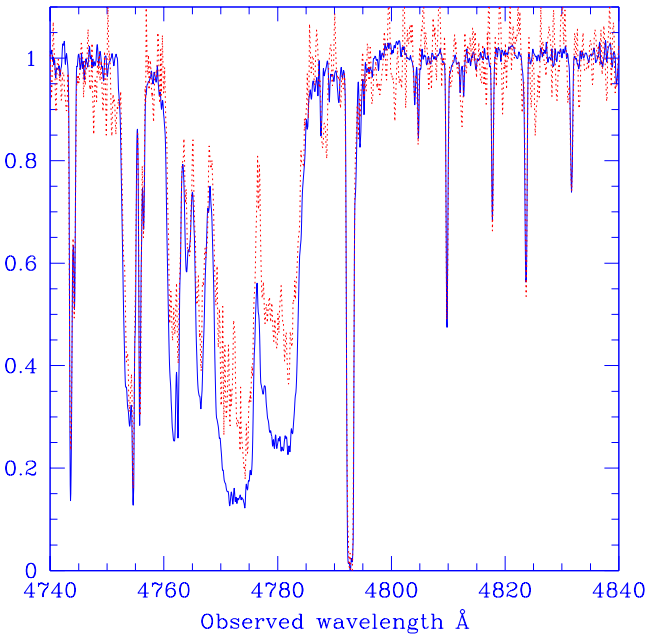


**Fig. 10.** Time variability of C IV absorption. The continuous line corresponds to our UVES data and the dotted line is the CASPEC spectrum from Lespine & Petitjean (1997). The resolution of the UVES spectrum is degraded to match that of the CASPEC data.

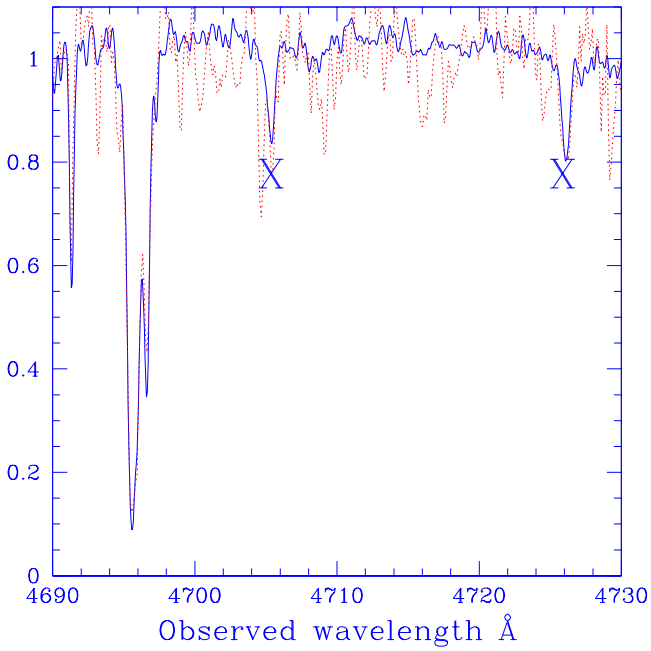


**Fig. 11.** Time variability of Si II absorption lines (marked with "X"). The solid line corresponds to the UVES data and the dotted line is the CASPEC data from Lespine & Petitjean (1997).

vary (see Fig. 11). The equivalent width ($w_{\rm r}$ = 0.18 Å) measured by Dinshaw & Impey (1997) is also consistent with what we measure.

If the variations are due to changes in the optical depth, then the variability time scale gives the recombination time scale. If the gas is highly ionized so that $n_{i+1} > n_i$, then the recombination time scale is given by

$$t_{\rm r} \;=\; \left(\frac{n_i}{n_{i+1}}\right) (n_{\rm e}\alpha_{i+1})^{-1} \qquad (7)$$

where, $n_i$ and $n_{i+1}$ are densities of species ionized $i-1$ and $i$ times and $\alpha_{i+1}$ is the recombination rate to the $i$ state (see e.g. Hamann et al. 1997). If the gas is less ionized, $n_i > n_{i+1}$, then

$$t_{\rm r} \;=\; (n_{\rm e}\alpha_i)^{-1}. \qquad (8)$$

Assuming C IV is the dominant ionization species and using the recombination cross-section for C IV given by Aldrovandi & Péquignot (1986) and Péquignot et al. (1991), the electron density, $n_{\rm e}$, is given by

$$n_{\rm e} \;\geq\; 4.2\times10^{3}\; T_4^{0.8}\; t_{\rm yr}^{-1}\;\; {\rm cm}^{-3}. \qquad (9)$$

Here, $T_4$ and $t_{\rm yr}$ are, respectively, the kinetic temperature in units of $10^4$ K and the elapsed time in years. It is therefore apparent that whatever the temperature of this gas is, the electronic density is quite large.

The comparison of covering factors estimated at two epochs (see Fig. 12) suggests that there could be some variation from one epoch to the other. However the $S/N$ ratio in our CASPEC spectrum, ∼10, implies an error of

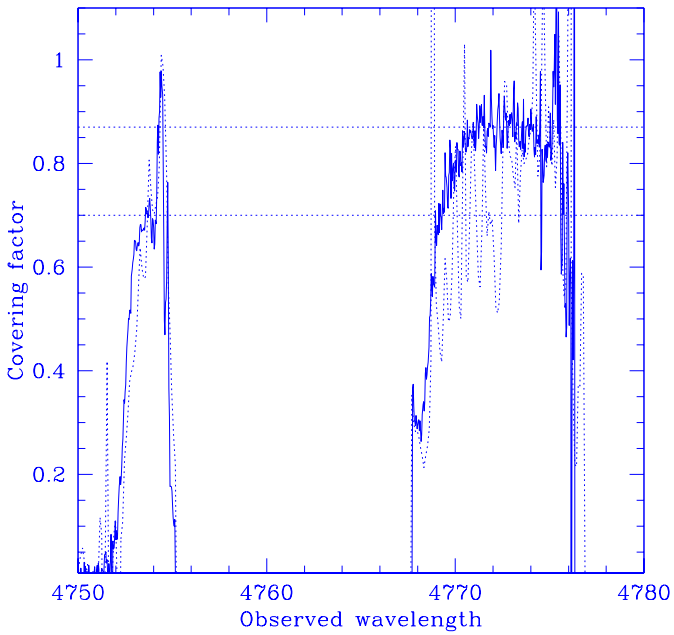


**Fig. 12.** Time variability of the covering factor of the C IV absorption lines. The solid line corresponds to the UVES data and the dotted line is the CASPEC spectrum from Lespine & Petitjean (1997).

up to 0.1 in the covering factor determination. Within this uncertainty we cannot ascertain the variation in the covering factor between the two epochs. Also there is no statistically significant difference in the covering factor of C IV absorption between UVES data and MMT data of Dinshaw & Impey (1996).

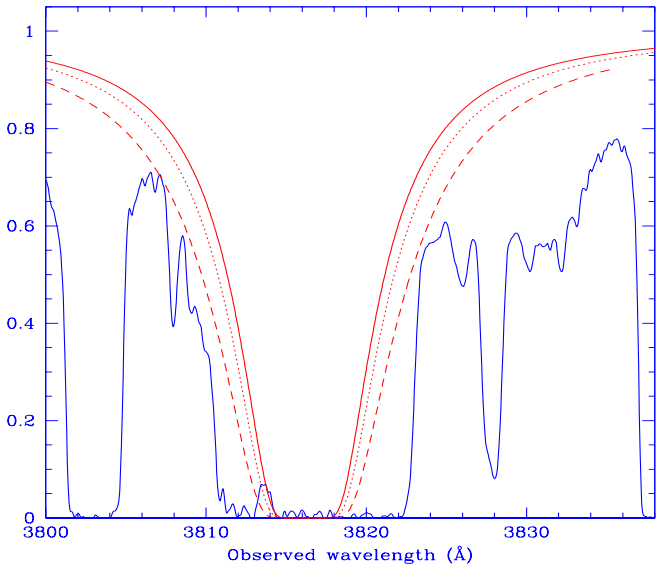


**Fig. 13.** Profile of the Lyman-$\alpha$ absorption line in the $z_{\rm abs} = 2.139$ system. As this part of the spectrum is affected by the BAL absorption the continuum was normalised using the spectrum of Q 1101-264. The solid, dotted and dashed curves are Voigt profiles for $\log N({\rm H\ I}) = 19.6$, 19.7 and 19.85 respectively. The residual flux at $\lambda = 3814$ Å suggests that $\log N({\rm H\ I}) \simeq 19.7$.

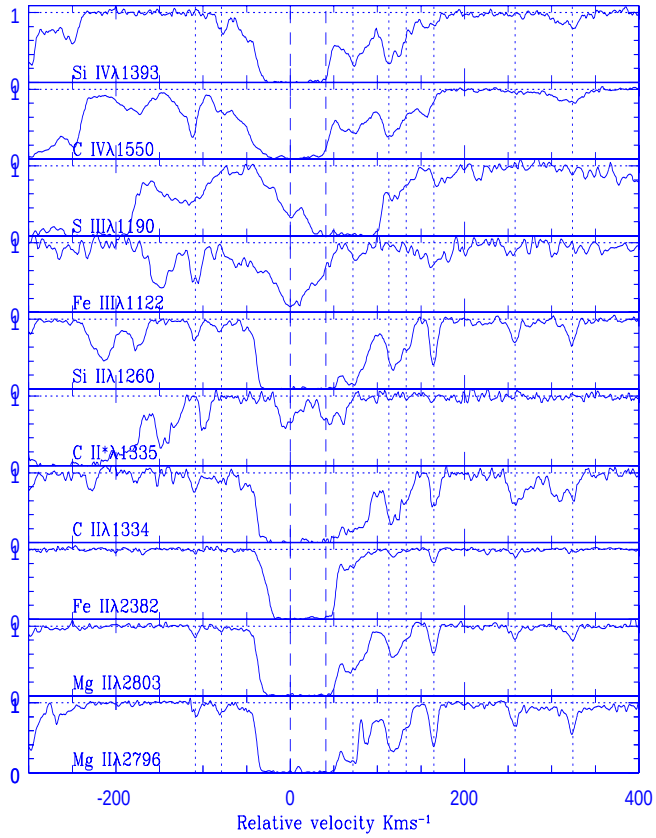


**Fig. 14.** Absorption profiles of some of the standard absorption lines in the $z_{\rm abs} = 2.139$ system. The dotted lines show the position of the weak narrow components. The dashed lines show the position of low ionization components discussed in the text.

It is possible that the relative increase in the C IV column density between years 1994 and 2000, $\geq$1.2, corresponds to a change of the C IV/C ratio and therefore a change in the ionization parameter. From the models by Hamann (1997) we derive that the gas has an ionization parameter $\log U$ of the order of $-1$ and that the increase in $N$(C IV) corresponds to a decrease of the ionization parameter by a factor larger than 2. This cannot be due to changes in the ionizing flux from the quasar as a change by $\sim$1 mag would have been noticed. It is also difficult to imagine that the distance of the cloud from the central ionizing source has increased by a factor 1.4. Thus the observed variation in the C IV profile could be either due to some non-equilibrium process or due to changes in the internal dynamics of the cloud. In order to understand the origin of the variability it is important to have a high resolution spectroscopic monitoring of this system.

## 5. The $z_{\rm abs} = 2.139$ system

### 5.1. Description of the system

Lespine & Petitjean (1997) derived an upper limit on the HI column density, $\log N({\rm H\ I}) < 4{\times}10^{19}$ cm$^{-2}$ from the absence of damping wings. As can be seen from Fig. 1, the Lyman-$\alpha$ absorption from this system is blended with the N V broad absorption at $z_{\rm abs} = 2.082$ system as well as the Si IV absorption from the $z_{\rm abs} = 1.72$ twin BAL systems. This means that the continuum is badly constrained. We have normalized the Tol 1037$-$2703 spectrum using the UVES data on Q 1101$-$264 as shown in Fig. 1. Although the possible damping wings are lost in the BALs, the residual flux at $\lambda \sim 3814$ Å (see Fig. 13) constraints the column density well. This feature is real as it is clearly visible in the two individual UVES exposures we have. We find that $19.6 < \log N({\rm H\ I}) < 19.8$ with a best fitted value of $\log N({\rm H\ I}) = 19.7$.

The Mg IIλ2797 absorption profile shows a strong component with narrow and weak satellites (marked with vertical dotted lines in Fig. 14) seen on both sides and spreading in total $\sim$430 km s$^{-1}$. This is a typical characteristic of the intervening Mg II systems. Interestingly, some of the narrow components exhibit Si II, C II and Fe II absorption lines with weak associated absorption lines of Si IV and C IV. When weaker transitions are considered, the strong feature splits into two main components of similar characteristics at $z_{\rm abs} = 2.1390$ and 2.1394 (marked with dashed vertical lines in Fig. 14). There are absorption lines at the expected positions of Fe IIIλ1122 and Si IIIλ1190. As these lines could be blended with intervening Lyman-$\alpha$ absorption lines, we derive upper limits on the corresponding column densities. The two strong components show detectable absorption from C I, N I, P II, Mg I, Mg II, S II, Ni II, Zn II, Cr II (see Fig. 15). As the above lines are weak, and in most of the cases multiplets are present, we could obtain reliable estimate of the column densities (see Table 1). The fact that all the saturated lines go to

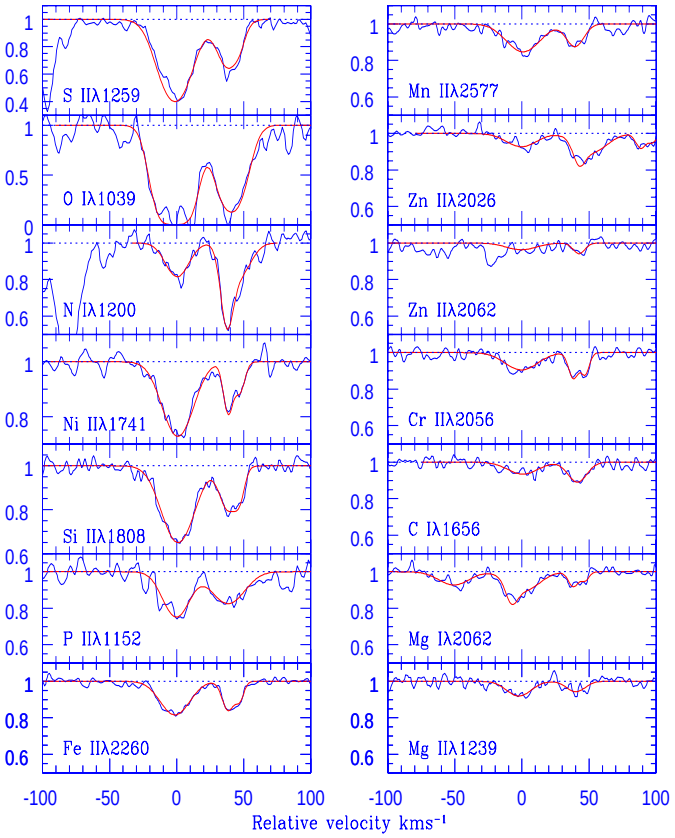


**Fig. 15.** Absorption profiles of few transitions in the $z_{\rm abs} = 2.139$ system. The Voigt profile fits are over-plotted.

zero and that Voigt profiles could be fitted consistently to the multiplets shows that the absorbing cloud completely covers the background source. This, together with the absence of absorption line variability and the presence of absorption due to C I strongly suggests that the physical conditions in this gas are very much similar to those prevailing in typical intervening damped Lyman-$\alpha$ system (see below).

Based on the absence of absorption from molecular hydrogen in the Lyman-band, we derive an upper limit of $10^{14}$ cm$^{-2}$ for the $H_2$ column density in both components and therefore, the molecular fraction $f = 2N(H_2)/(2N(H_2) + N(H\ I)) < 8 \times 10^{-6}$. As shown by Petitjean et al. (2000), such low value is probably consequence of high temperature ($T > 3000$ K) in diffuse gas.

We estimate the upper limit on $N$(C I$^*$) using a combined spectrum obtained by stacking the regions centered at rest wavelengths 1277.28, 1277.51, 1329.08, 1329.10, 1329.12, 1560.68, 1560.71, 1656.26, 1657.38 and 1657.91 Å. There are coincident absorption features at the expected position of C II$^*$ for both components at $z_{\rm abs} = 2.1390$ and 2.1394 (see Fig 14). The C II$^*$ absorption at $z_{\rm abs} = 2.1390$ is probably (at least partly) blended with C IIλ1334 from a narrow component at 258 km s$^{-1}$ seen in Mg II. The C II$^*$ absorption at $z_{\rm abs} = 2.1394$ has two sub-components. The red one is blended with C IIλ1334 at 323 km s$^{-1}$, the other one at $z_{\rm abs} = 2.1394$ is free of blending. From the fact that the C IIλ1036 line is saturated we obtain a lower limit $N$(C II) $> 3\times10^{14}$ cm$^{-2}$.

**Table 1.** Column densities (in cm$^{-2}$) and metallicities relative to solar.

| Species | $z_{\rm abs} = 2.1390$ | $z_{\rm abs} = 2.1394$ | [X/H][a] |
|---|---|---|---|
| H I | $5 \times 10^{19}$ | | |
| $H_2$ | $<10^{14}$ | | |
| C I | $3.26 \pm 0.17 \times 10^{12}$ | $3.05 \pm 0.17 \times 10^{12}$ | |
| C I$^*$ | $\leq 3 \times 10^{12}$ | $\leq 2 \times 10^{12}$ | |
| C II$^*$ | ..... | $2.03 \pm 0.01 \times 10^{13}$ | |
| C II | $\geq 3 \times 10^{14}$ | $\geq 3 \times 10^{14}$ | |
| N I | $3.05 \pm 0.20 \times 10^{13}$ | $7.17 \pm 0.58 \times 10^{13}$ | $-1.66$ |
| O I | $>6.54 \pm 0.12 \times 10^{15}$ | $1.86 \pm 0.12 \times 10^{15}$ | $>-0.64$ |
| Mg I | $4.85 \pm 0.22 \times 10^{12}$ | $1.68 \pm 0.22 \times 10^{12}$ | |
| Mg II | $2.15 \pm 0.51 \times 10^{15}$ | $\leq 1 \times 10^{15}$ | $+0.05$ |
| Si II | $1.23 \pm 0.01 \times 10^{15}$ | $4.60 \pm 0.03 \times 10^{14}$ | $-0.02$ |
| P II | $9.41 \pm 0.58 \times 10^{12}$ | $7.82 \pm 0.62 \times 10^{12}$ | $-0.03$ |
| S II | $4.84 \pm 0.26 \times 10^{14}$ | $1.70 \pm 0.43 \times 10^{14}$ | $-0.15$ |
| S III | $\leq 4 \times 10^{14}$ | $\leq 1 \times 10^{15}$ | |
| Cr II | $3.90 \pm 0.17 \times 10^{12}$ | $3.20 \pm 0.25 \times 10^{12}$ | $-0.53$ |
| Cr III | $\leq 3 \times 10^{12}$ | $\leq 2 \times 10^{12}$ | |
| Mn II | $2.12 \pm 0.05 \times 10^{12}$ | $8.96 \pm 0.38 \times 10^{11}$ | $-0.75$ |
| Fe II | $2.40 \pm 0.06 \times 10^{14}$ | $1.20 \pm 0.09 \times 10^{14}$ | $-0.65$ |
| Fe III | $\leq 4 \times 10^{14}$ | $\leq 5 \times 10^{13}$ | |
| Ni II | $1.85 \pm 0.03 \times 10^{13}$ | $6.15 \pm 0.36 \times 10^{12}$ | $-0.56$ |
| Zn II | $7.57 \pm 0.48 \times 10^{11}$ | $4.72 \pm 0.60 \times 10^{11}$ | $-0.26$ |

[a]Metallicity relative to solar,
[X/H] = log $(N(X)/N(H)]-\log(N(X)/N(H))_\odot$.

### 5.2. Chemical enrichment

In what follows we use the standard defition [X/H] = log $(N(X)/N(H)]-\log(N(X)/N(H))_\odot$ and the solar metallicities given by Savage & Sembach (1996).

Before discussing the chemical composition of the gas, one has to worry about potential ionization corections especially for a cloud with log $N$(H I) $\sim 19.7$. From Table 1, it can be seen that $N$(Cr III)/$N$(Cr II) $< 0.77$ and 0.63 and $N$(Fe III)/$N$(Fe II) $< 1.7$ and 0.42 in the two components respectively. As the two components have otherwise similar characteristics, we can conclude that most of the metals are in the singly ionized state. Howk & Sembach (1999) have shown that if $N$(Fe III)/$N$(Fe II) $< 1$, the ionization correction for relative metallicity is negligible for all species of interest here. Absolute metallicities could be slightly *underestimated* but by no more than a factor of two.

Zinc metallicity is of the order of 0.5 solar. The consistent and mild depletion (of about a factor of two) of Fe, Cr and Ni compared to Zn is suggestive of small amounts of dust if any. The four $\alpha$-elements Mg, Si, P, and S have consistent metallicities slightly larger (by about a factor of two) than the Zn metallicity. Note however that sulphur has slightly smaller metallicity compared to the other $\alpha$-elements. Given the uncertainties involved in nucleosynthesis models, it is difficult, if not impossible, to draw any

conclusion from one measurement. However it is interesting to note that such an abundance pattern is commonly seen in damped Lyman-$\alpha$ systems (see e.g. Lu et al. 1996) apart from the fact that the system toward Tol 1037−2703 is the damped system of highest metallicity at such redshift. In addition, the nitrogen abundance is quite small, [N/Zn] = −1.3, [N/S] = −1.5. This is broadly consistent with nitrogen being produced as a secondary element in massive stars with little contribution from the primary production that occurs in intermediate mass stars (3–8 $M_{\odot}$). If true, this means the star formation in this system was intense and has proceeded very quickly through the formation of massive stars. However, it is surprizing to find such low [N/Zn] = −1.3 ratio when [Zn/H] = −0.3 (see e.g. Centurion et al. 1998). Note that H I and N I are tied up by charge exchange reaction. Although one can question the charge exchange reaction rate between hydrogen and nitrogen, especially if the temperature of the gas is high, it seems difficult to explain the low N I/H I ratio by ionization effects only (see also Viegas 1995). Finally, it is most interesting to note that the abundance pattern in the $z_{\rm abs} = 2.139$ system is close to what is observed in the Magellanic Bridge (Lehner et al. 2001) whereas the column densities are similar to those in the Weak Low Velocity (WLV) gas toward 23 Orionis (see Welty et al. 1999) except for N I which is much stronger toward 23 Ori. This could suggest again that this damped Lyman-$\alpha$ system arises in halo-like gas rather than through a typical galaxy disk.

### 5.2.1. Discussion

The detection of C I in this system is confirmed by the presence of lines with $\lambda_{\rm rest}$ = 1650 and 1560 Å. C I has been detected only in few of the intervening damped Lyman-$\alpha$ systems [$z_{\rm abs}$ = 1.776 toward Q 1331+170 (Songaila et al. 1994); $z_{\rm abs}$ = 1.97 toward Q 0013-00 (Ge et al. 1997); $z_{\rm abs}$ = 1.6748 toward PKS 1756+237 (Roth & Bauer 1999); $z_{\rm abs}$ = 2.337 toward PKS 1232+0815 (Srianand et al. 2000)]. Apart from the system toward PKS 1756+237 (where reliable estimate of the HI column density is not possible due to poor $S/N$ in the spectrum) all other systems are confirmed high column density DLAs. The detection of C I toward Tol 1037−2703 is therefore a consequence of the high metallicity of the system.

Assuming that the carbon abundance is similar to that of silicon and that C II is the dominant ionization state we derive a conservative upper limit on the C II column density to be $1.6\times10^{15}$ cm$^{-2}$ in the $z_{\rm abs} = 2.1394$ component. Using the measured column density of C II* and assuming collisional excitation and radiative deexcitation of the fine−structure level we determine a range of electron density,

$$n_{\rm e} \;=\; (0.48 - 2.57)\; T_4^{0.5}\; \exp[91.25/T]. \qquad (10)$$

Assuming photo-ionization equilibrium between C I and C II and using the atomic data from Shull & Van Streenberg (1982), we can write,

$$n_{\rm e} \;=\; (0.82 - 4.42) \times 10^9\; T_4^{0.64}\; \Gamma, \qquad (11)$$

where $\Gamma$ is the photo-ionization rate. From the above two equations, it can be seen that $\Gamma = (0.11 - 4.73) \times 10^{-9}$ s$^{-1}$ for a temperature in the range $10^3$−$10^4$ K. In the local ISM, $\Gamma \sim 2-3.3\times10^{-10}$ (Péquignot & Aldrovandi 1986). Thus the deduced ambient UV flux in these components is consistent with or slightly larger than that in the ISM of our Galaxy.

Similarly from Mg I and Mg II column densities, we obtain

$$n_{\rm e} \;\geq\; 2.0 \times 10^9\; T_4^{0.89}\; \Gamma. \qquad (12)$$

The allowed value of $\Gamma$ is $\leq 3.02 \times 10^{-9}$ when the value in the Galactic ISM is $\Gamma = 5.7$−$8.0 \times 10^{-11}$. This is consistent with the previous conclusion. Note that the hydrogen ionizing background radiation from quasars and galaxies (Haardt & Madau 1996) is about two orders of magnitude smaller than that seen in our galactic ISM and an additional source of UV flux is needed. This could be Tol 1037−2703 itself as the quasar is able to provide the additional flux even if the gas is at a distance ∼few Mpc from the QSO.

It is known that the fine structure lines of C I can be excited by the cosmic microwave background radiation (Bahcall & Wolf 1968; Meyer et al. 1986) and therefore can be used to constrain its temperature. Assuming the CMBR pumping to be the only excitation mechanism we obtain an upper limit on the temperature of the background to be 16.4 and 13.2 K for $z_{\rm abs} = 2.1390$ and 2.1394 components respectively (see Srianand et al. 2000 for details on the derivation). These limits are consistent with the value of 8.6 K expected in the framework of standard hot Big-Bang cosmology.

## 6. Summary

We report the detection of three BAL systems at $z_{\rm abs} = 1.5181$, 1.7018 and 1.7569 toward Tol 1037−2703. These systems have apparent ejection velocity of, respectively, 36 000, 25 320, and 22 315 km s$^{-1}$ with respect to the accurate emission redshift ($z_{\rm em}$ = 2.201) we measure using the Mg II emission line. The identification of the former BAL is based on Mg I, Mg II, Fe II and Al II absorptions and the system belongs to the class of low ionization Mg II BALs. The latter two systems are typical high-ionization BALs with absorptions from N V and C IV and no low-ionization lines. Thus Tol 1037−2703 is unique in the sense that this is the only QSO known that shows well detached BALs with widely differing ionization conditions. Broadness of the profiles and inferred covering factors suggest that the projected size of the corresponding absorbing clouds is less than that of the UV continuum emitting region.

We show, using C IV and Al III doublets, that the gas responsible for the $z_{\rm abs} = 2.082$ system does not cover the background source of continuum completely. Spectra of Tol 1037−2703 obtained at two different epochs, separated by ∼2 yrs in the rest frame of the QSO, suggests variability of the C IV absorption. The relative strength of the fine-structure lines due to Si II and C II is a consequence of excitation by a strong IR source, probably associated with the quasar. Similar properties have been derived in the case of the $z_{\rm abs} = 3.8931$ system toward APM 08279+5255 (Srianand & Petitjean 2000). We note that the covering factor for C IV, $f_{\rm c} \sim 0.86$, is constant over the velocity range span by the absorption line. The covering factor estimated for Al III, $f_{\rm c} \sim 0.3$, is much less, confirming the findings by Petitjean & Srianand (1999) that the covering factor is increasing with increasing ionization state.

We report the detection of weak low-ionization lines such as C I, Zn II, Cr II, Ni II, P II and S II in the moderately damped ($\log N$(H I) = 19.7) $z_{\rm abs}$ 2.139 system. These lines are detected in two components at $z_{\rm abs}$ 2.1390 and 2.1394. The absolute metallicity is close to solar with [Zn/H] = −0.26. The $\alpha$-chain elements have metallicities consistently solar (respectively +0.05, −0.02, −0.03 and −0.15 for [Mg/H], [Si/H], [P/H] and [S/H]) and iron peak elements are depleted by a factor of about two ([Fe/Zn], [Cr/Zn], [Mn/Zn] and [Ni/Zn] are equal to −0.39, −0.27, −0.49, −0.30). It is noticeable that the pattern is similar to what is seen in standard damped Lyman-$\alpha$ systems (Lu et al. 1996). However, in the case of Tol 1037−2703, not only is the metallicity high but also the nitrogen abundance is small, [N/Zn] = −1.40, which is difficult to understand in standard nucleosynthesis models. Such a metallicity pattern is seen, however, in the Magellanic Bridge (Lehner et al. 2001). This clearly indicates that the period of intense star formation activity in this system has lasted for less than 0.5 Gyr and that metals have primarily been produced by massive stars. Using the C II* column density and the Mg I/Mg II and C I/C II ratios, we show that the required photo-ionization rates are higher than expected if the gas is ionized by the UV background and some extra source of ionization is needed. Assuming that the QSO is the ionizing source implies that the absorbing gas is situated ∼few Mpc away from it. The high metal enrichment, within a few Mpc from a QSO that, in addition, shows a large variety of outflowing gas might suggest an association of this gas with the QSO. It is possible that this absorbing gas has in common with the quasar a period of intense star formation and/or has been ejected from the QSO a few $10^8$ yrs ago.

Using the limits on the C I* column density and assuming excitation is due to CMBR photons we obtain an upper limit on the temperature of the cosmic microwave background of 16.2 and 13.2 K respectively for these components. These limits are consistent with the expected temperature of 8.6 K in the framework of standard hot Big−bang cosmology.

*Acknowledgements.* We thank Cédric Ledoux for a careful reduction of the spectrum and Chris Impey for sharing with us a 1994 MMT spectrum. We gratefully acknowledge support from the Indo-French Centre for the Promotion of Advanced Research (Centre Franco-Indien pour la Promotion de la Recherche Avancée) under contract No. 1710-1. RS thanks IAP for hospitality during the time part of this work was completed.

## References

Aldrovandi, S. M. V., & Péquignot, D. 1973, A&A, 25, 137
Bahcall, J. N., & Wolf, R. A. 1968, ApJ, 152, 701
Becker, R. H., White, R. L., Gregg, M. D., et al. 2000, ApJ, 538, 72.
Centurión, M., Bonifacio, P., Molaro, P., & Vladilo, G. 1998, ApJ, 509, 520
Cristiani, S., Danzinger, I. J., & Shaver, P. A. 1987, MNRAS, 227, 639
de Kool, M., Arav, N., Becker, R. H., et al. 2001, ApJ, 548, 609
Dinshaw, N., & Impey, C. D. 1996, ApJ, 458, 73
D'Odorico, S., et al. 2000, SPIE, 4005, 121
Elvis, M., Wilkes, B. J., McDowell, J. C., et al. 1994, ApJS, 95, 1
Espey, B. R., Carswell, R. F., Bailey, J. A., Smith, M. G., & Ward, M. 1989, ApJ, 342, 666
Gaskell, C. M. 1982, ApJ, 263, 79
Jian Ge, Bechtold, J., & Black, J. H. 1997, ApJ, 474, 67
Haardt, F., & Madau, P. 1996, ApJ, 461, 20
Hamann, F., 1997 ApJS, 109, 279
Hamann, F., Barlow, T. A., & Junkkarinen, V. 1997, ApJ, 478, 87
Howk, J. C., & Sembach, K. R. 1999, ApJ, 523, L141
Jakobsen, P., et al. 1986, ApJ, 303, L27
Lehner, N., Sembach, K. R., Dufton, P. L., Rolleston, W. R. J., & Keenan, F. P. 2001 [astro-ph/0101548]
Lespine, Y., Petitjean, P. 1997, A&A, 317, 416
Lu, L., Sargent, W. L, W., Womble, D. S., & Barlow, T. A. 1996, ApJS, 107, 475
Meyer, D. M., Black, J. H., Chaffee, F. H., Foltz, C. B., & York, D. G. 1986, ApJ, 308, L37
Péquignot, D., & Aldrovandi, S. M. V. 1986, A&A, 161, 169
Péquignot, D., Petitjean, P., & Boisson, C. 1991, A&A, 251, 680
Petitjean, P., Rauch, M., & Carswell, R. F. 1994, A&A, 291, 29
Petitjean, P., & Srianand, R. 1999, A&A, 345, 73
Petitjean, P., Srianand, R., & Ledoux, C. 2000, A&A, 364, L26
Robertson, J. G. 1987, MNRAS, 227, 653
Roth, K. C., & Bauer, J. M. 1999, ApJ, 515, L57
Savage, B. D., & Sembach, K. R. 1996, ARA&A, 34, 279
Sargent, W. L. W., & Steidel, C. C. 1987, ApJ, 322, 142
Shull, M. J., & Van Steenberg, M. E. 1982, ApJS, 48, 95
Songaila, A., et al. 1994, Nature, 371, 43
Srianand, R., & Petitjean, P. 2000, A&A, 357, 414
Srianand, R., Petitjean, P., & Ledoux, C. 2000, Nature, 408, 931
Srianand, R., & Shankaranarayanan, S., 1999, ApJ, 518, 672
Telfer, R. C., Kriss, G. A., Zheng, W., Davidsen, A. F., & Green, R. F. 1999, ApJ, 509, 132
Ulrich, M. H., & Perryman, M. A. C. 1986, MNRAS, 220, 429
Viegas, S. M. 1995, MNRAS, 276, 268
Voit, G. M., Weymann, R. J., & Korista, K. T. 1993, ApJ, 413, 95
Welty, D. E., Hobbs, L. M., Lauroesch, J. T., et al. 1999, ApJS, 124, 465